

Robust Modeling of Constant Mean Curvature Surfaces

Hao Pan¹

Yi-King Choi¹

Konrad Polthier⁴

Yang Liu²

Caiming Zhang⁵

Wenchoao Hu¹

Qiang Du³

Wenping Wang¹

¹The University of Hong Kong

²Microsoft Research Asia

³Pennsylvania State University

⁴Freie Universität Berlin

⁵Shandong University

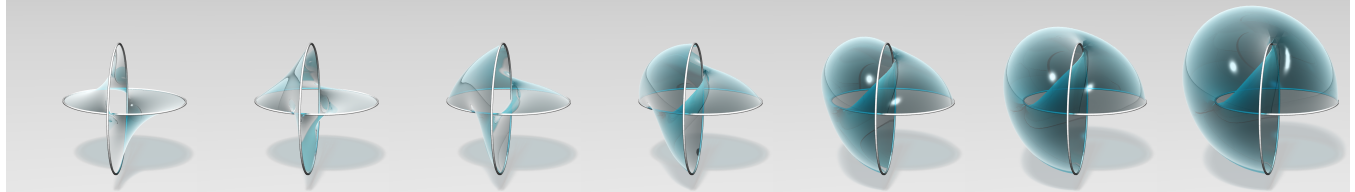


Figure 1: A series of CMC surfaces with the same boundary of two interlaced rings. They are generated with our method by increasing a parameter t that controls the force imposed on the surface and thereby achieving different surface curvatures. The first one is a minimal surface with $t = 0$.

Abstract

We present a new method for modeling discrete constant mean curvature (CMC) surfaces, which arise frequently in nature and are highly demanded in architecture and other engineering applications. Our method is based on a novel use of the CVT (*centroidal Voronoi tessellation*) optimization framework. We devise a CVT-CMC energy function defined as a combination of an extended CVT energy and a volume functional. We show that minimizing the CVT-CMC energy is asymptotically equivalent to minimizing mesh surface area with a fixed volume, thus defining a discrete CMC surface. The CVT term in the energy function ensures high mesh quality throughout the evolution of a CMC surface in an interactive design process for form finding. Our method is capable of modeling CMC surfaces with fixed or free boundaries and is robust with respect to input mesh quality and topology changes. Experiments show that the new method generates discrete CMC surfaces of improved mesh quality over existing methods.

CR Categories: I.3.5 [Computer Graphics]: Computational Geometry and Object Modeling—Geometric algorithms, languages, and systems

Keywords: surface modeling, constant mean curvature, mesh quality, centroidal Voronoi tessellation

Links: DL PDF

ACM Reference Format

Pan, H., Choi, Y., Liu, Y., Hu, W., Du, Q., Polthier, K., Zhang, C., Wang, W. 2012. Robust Modeling of Constant Mean Curvature Surfaces. *ACM Trans. Graph.* 31, 4, Article 85 (July 2012), 11 pages.
DOI = 10.1145/2185520.2185581 <http://doi.acm.org/10.1145/2185520.2185581>

Copyright Notice

Permission to make digital or hard copies of part or all of this work for personal or classroom use is granted without fee provided that copies are not made or distributed for profit or direct commercial advantage and that copies show this notice on the first page or initial screen of a display along with the full citation. Copyrights for components of this work owned by others than ACM must be honored. Abstracting with credit is permitted. To copy otherwise, to republish, to post on servers, to redistribute to lists, or to use any component of this work in other works requires prior specific permission and/or a fee. Permissions may be requested from Publications Dept., ACM, Inc., 2 Penn Plaza, Suite 701, New York, NY 10121-0701, fax +1 (212) 869-0481, or permissions@acm.org.
© 2012 ACM 0730-0301/2012/08-ART85 \$15.00 DOI 10.1145/2185520.2185581
<http://doi.acm.org/10.1145/2185520.2185581>

1 Introduction

Constant Mean Curvature (CMC) surfaces arise widely as natural or man made structures. Soap bubbles are CMC surfaces with nonzero constant mean curvature and soap films are special CMC surfaces with zero mean curvature, called *minimal surfaces*. Tensile membrane structures in architecture can be modeled as minimal surfaces [Brew and Lewis 2003a]. Pneumatic architectures, including inflatable domes and enclosures, are modeled as CMC surfaces as well [Smith 2003]. CMC surfaces have received much attention in mathematics, with the goal to find new types of CMC surfaces by employing the properties of symmetry, periodicity and so on.

Modeling CMC surfaces is an active research problem in shape modeling. Computationally practical approaches to modeling CMC surfaces try to find a discrete approximation, most commonly in the form of a triangle mesh, to a CMC surface by optimizing some energy function. For example, a CMC surface can be computed as a minimizer of the surface area functional subject to the constraint of some fixed volume. This characterization of CMC surfaces has given rise to several methods that compute CMC surfaces by solving a constrained optimization problem on a mesh surface.

A mesh surface is defined by mesh vertices and mesh connectivity, i.e., edges connecting the vertices. When using a mesh surface for shape representation, two main criteria of mesh quality are the distribution of mesh vertices and edge connectivity. High quality meshes, in terms of mesh smoothness and the shape of face elements, are desired in many geometric processing tasks, such as numerical simulation and estimation of differential surface properties.

Poor mesh quality is a major issue with existing methods for modeling CMC surfaces. These methods lack a mechanism of optimizing mesh connectivity. Typically, such a method drives an initial mesh to a final shape by updating only the positions of mesh vertices while keeping the same edge connectivity of the initial mesh. As a result, the final mesh is often a poor representation of the true CMC surface intended due to the presence of poorly shaped face elements [Brew and Lewis 2003b]. Improvement of mesh connectivity via remeshing could be performed with user assistance or as post-processing, but such an operation is neither automatic nor consistent with the original energy minimization principle. Hence, currently there is a lack of a unified and automatic method that can optimize both vertex positions and edge connectivity in a consistent

manner for modeling high quality discrete CMC surfaces.

Contributions. We propose a new method for modeling CMC surfaces that optimizes both the mesh vertices and edge connectivity consistently by minimizing a novel energy function. This energy is a combination of an extended CVT (centroidal Voronoi tessellation) energy on a moving mesh surface and a volume functional. We show that the minimizer of this new energy function is a CMC surface with high mesh quality, as enforced by the CVT energy term. We present an efficient numerical method for minimizing the new energy function. Because of its inherent capability of optimizing edge connectivity, our method maintains good mesh quality for dynamic CMC surfaces during interactive design of CMC surfaces. The method is capable of modeling CMC surfaces without boundaries, as well as those with free or fixed boundaries. It is robust against radical changes of surface topology and shape. Experiments show that this method generates discrete CMC surfaces of better quality than by the existing methods.

2 Related Work

CMC surfaces. New CMC surfaces can be discovered using fundamental patches and the properties of symmetry and periodicity. See [Kapouleas 1990] for an introduction to various mathematical techniques for constructing new CMC surfaces. Oberknapp and Polthier [1997] reduce the problem of CMC surface computation in \mathbb{E}^3 to the problem of minimal surface computation in \mathbb{S}^3 . However, it is unclear how these methods can be implemented for modeling CMC surfaces complying with a specified boundary, as required for surface modeling in many applications.

Discrete representations, especially triangle meshes, are commonly used by practical methods for computing and representing CMC surfaces. A CMC surface is characterized as a surface minimal area with a fixed enclosed volume. Several methods have been proposed in the literature that apply this characterization to computing a discrete CMC surface in the form of a triangle mesh. Brakke [1992] computes a CMC surface by minimizing a functional defined as the sum of mesh surface area and a multiple of volume enclosed by the surface. Similarly, Polthier and Rossman [2002] define a discrete CMC surface by equalizing mesh surface area gradient and volume gradient with respect to mesh vertices. Smith [2003] instead minimizes the area of a mesh surface subject to the constraint of observing specified mean curvature on the mesh. Dziuk and Hutchinson [2006] use FEM to optimize the energy functional of surface area plus a variable volume term to compute a surface with variable mean curvature. Xu and Zhang [2008] compute CMC surfaces by solving a geometric PDE defined on mesh surfaces. Most of these methods assume a reasonable good initial mesh and are not concerned about the mesh quality in terms of edge connectivity.

Similar to the approach taken by [Brakke 1992], [Polthier and Rossman 2002] and [Dziuk and Hutchinson 2006], our formulation is also built upon characterizing a CMC surface as a minimizer of surface area subject to the volume constraint. However, unlike these methods that minimize only surface areas, we devise a novel functional whose minimization optimizes both mesh surface area and mesh connectivity in a consistent and unified manner. Our method therefore yields high quality discrete CMC surfaces.

Minimal surfaces. Minimal surfaces, having zero mean curvature at every point, are a special case of CMC surfaces. There is considerable amount of research on minimal surfaces. Computation of minimal surfaces with a given boundary of disk topology normally works by minimizing the surface area while maintaining the boundary condition. Naturally, methods for modeling CMC sur-

faces can also be used to model minimal surfaces. Other approaches to computing minimal surfaces include minimization of mesh area using mean curvature flow in the form of geometric PDEs by Xu et al. [2006], and minimization of the Dirichlet energy by Pinkall and Polthier [1993]. Our method is also capable of generating discrete minimal surfaces of better mesh quality than by other existing methods.

CVT. We now give a brief review on centroidal Voronoi tessellations (CVTs). A thorough survey on CVTs can be found in [Du et al. 1999] and [Du et al. 2010]. Given a set $X = \{x_1, \dots, x_k\}$ of k seed points in a compact domain $\Omega \subset \mathbb{E}^d$, the Voronoi cell V_i associated with a seed point x_i is the set of points in Ω which are closer to x_i than any other seed points, that is, $V_i = \{y \in \Omega \mid \|y - x_i\| \leq \|y - x_j\|, \forall j \neq i, j = 1, \dots, k\}$. The collection of all Voronoi cells $\{V_i\}_{i=1}^k$ forms a partition of Ω for which we call a *Voronoi tessellation*. A CVT is a special kind of Voronoi tessellation in which every seed point coincides with the centroid of its corresponding Voronoi cell.

Equivalently, a CVT is characterized by a critical point of the CVT energy function [Du et al. 1999]:

$$F_{\text{CVT}}(X) = \sum_{i=1}^k \int_{y \in V_i} \rho(y) \|y - x_i\|^2 d\sigma, \quad (1)$$

where $\rho(\cdot)$ is a density function defined over Ω and $d\sigma$ is the differential volume element of Ω . Therefore, a CVT can be obtained by computing a local minimizer of $F_{\text{CVT}}(X)$. Liu et al. [2009] show that, under some assumptions about the domain Ω and the density function ρ , the CVT function $F_{\text{CVT}}(X)$ in Eq. (1) is C^2 . Hence, they propose to compute CVTs using L-BFGS, a quasi-Newton method, which is much faster than the conventional Lloyd's method [Du et al. 1999].

When the domain Ω is a surface embedded in 3D space \mathbb{E}^3 , a Voronoi cell V_i is the intersection of Ω with all the half spaces determined by the bisectors of the seed point x_i and the other seed points. Such a tessellation of the surface is called a *restricted Voronoi diagram* (RVD) [Du et al. 2003], and its dual is called a *restricted Delaunay tessellation* (RDT). Yan et al. [2009] propose a method for fast computation of RVDs and CVTs on meshes for the purpose of surface remeshing.

As CVTs tend to generate uniformly distributed points, they have found many applications in geometric processing and computer graphics. However, to the best of our knowledge, although CVTs restricted to surfaces have been discussed in [Du et al. 2003], they have not been applied previously to surface modeling. We will show how the CVTs can be used for modeling discrete CMC surfaces.

3 New Variational Formulation of CMC Surfaces

3.1 Existing formulation

Since a CMC surface S is a minimizer of surface area subject to a volume constraint, a general approach to computing a CMC surface satisfying some boundary conditions is to minimize the functional $\text{Area}(S) + \lambda \times \text{Vol}(S)$, where $\text{Area}(S)$ is the surface area of S , $\text{Vol}(S)$ is its enclosed volume¹, λ is some parameter controlling the shape of the surface. Let S_0 be a surface that is a minimizer of this

¹From a local point of view, the formula refers to the area of a small neighborhood \mathcal{N} around a point and the volume enclosed by the cone de-

functional. Then, by the Lagrange principle for constrained minimization, S_0 has the minimum area among all the surfaces having the same volume of S_0 . Hence, S_0 is a CMC surface.

When the surface S is a mesh surface, the above functional takes the form

$$\tilde{F}(\mathcal{P}) = \tilde{F}_{\text{Area}}(\mathcal{P}) + \lambda \tilde{F}_{\text{Vol}}(\mathcal{P}), \quad (2)$$

where \mathcal{P} is the vertex set of the mesh with some fixed mesh connectivity, $\tilde{F}_{\text{Area}}(\mathcal{P})$ the mesh area, and $\tilde{F}_{\text{Vol}}(\mathcal{P})$ the volume enclosed by the mesh. A minimizer of this function is then a discrete CMC surface. This is the approach followed by Brakke [1992] and Polthier and Rossman [2002], for example. This approach can be used for interactive modeling of CMC by varying the value of λ , which is equivalent to specifying the mean curvature. A major problem with the functional $\tilde{F}(\mathcal{P})$ in Eq. (2) is that it does not take into account the optimization of mesh connectivity and therefore fails to reflect mesh quality.

3.2 CVT energy vs. surface area

In view of the need to improve mesh quality, we note the capability of the CVT (centroidal Voronoi tessellation) in uniformly distributing mesh vertices and optimizing mesh connectivity using Delaunay triangulation. The main idea behind our method is to replace the surface area term in the preceding formulation of CMC surfaces by the CVT energy term. Therefore, the key now is to demonstrate that, when minimizing the CVT energy on a variable mesh surface, the surface area is minimized. To this end, we will now prove that the CVT energy of a CVT on a mesh surface Ω in \mathbb{E}^3 is asymptotically proportional to the squared area of Ω .

Let Ω be a surface patch of finite area $|\Omega|$ in \mathbb{E}^3 , with constant density $\rho = 1$. Given a set of seed points $X = \{x_i\}_{i=1}^N \subset \Omega$, the CVT energy of Ω with respect to X is

$$E = \sum_{i=1}^N \int_{V_i} \|x - x_i\|^2 d\sigma = \sum_{i=1}^N E_i, \quad (3)$$

where N is the number of seed points, $\|\cdot\|$ the Euclidean distance in \mathbb{E}^3 , and E_i the energy of the Voronoi cell of x_i .

Consider a CVT of the surface Ω , which is a minimizer of the functional in Eq. (3). According to Gersho's conjecture [Gersho 1979] (proved by Gruber [2001] for Riemannian 2-manifolds), when $N \rightarrow \infty$, the following two properties hold for a CVT asymptotically:

G1. *Energy equipartition:* $E_i = \frac{E}{N}$.

G2. *Cell congruency:* All the Voronoi cells are congruent to the same regular hexagon.

Now we are going to derive the relation between the CVT energy E and the surface area $|\Omega|$. Let h denote the edge length of the limit Voronoi cells, which are congruent regular hexagons. On one hand, since E_i is an integral of square distance times the area element over the Voronoi regions, we have

$$E_i = \int_{V_i} \|x - x_i\|^2 d\sigma = \tau h^4 + O(h^5),$$

where $\tau = \frac{5\sqrt{3}}{8}$. By property **G1**, it follows that

$$E = \tau N h^4 + N \times O(h^5). \quad (4)$$

defined by a fixed arbitrary point in \mathbb{E}^3 and the boundary of \mathcal{N} [Polthier and Rossman 2002].

On the other hand, by property **G2**, there is

$$|V_i| = \tau' h^2 + O(h^3),$$

where $\tau' = \frac{3\sqrt{3}}{2}$. Since $\sum_{i=1}^N |V_i| = |\Omega|$, we obtain

$$|\Omega| = \tau' N h^2 + N \times O(h^3). \quad (5)$$

Combining Eqs. (4) and (5) yields

$$E = \frac{\tau}{\tau'^2} \times \frac{|\Omega|^2}{N} + N \times O(h^5), \quad (6)$$

From Eq. (5), we have $h = |\Omega|^{1/2} \times O(N^{-1/2})$. It follows that $N \times O(h^5) = |\Omega|^{5/2} \times O(N^{-3/2})$. Therefore, from Eq. (6) we have

$$E = \frac{\tau}{\tau'^2} \times \frac{|\Omega|^2}{N} + |\Omega|^{5/2} \times O(N^{-3/2}), \quad \text{or}$$

$$N \times E = \frac{\tau}{\tau'^2} |\Omega|^2 + |\Omega|^{5/2} \times O(N^{-1/2}). \quad (7)$$

Hence, we conclude that the scaled CVT energy for a CVT, i.e., $N \times E$, is asymptotically proportional to the squared surface area $|\Omega|^2$ as the number of seed points N goes to infinity.

3.3 Extended CVT energy

Let $\mathcal{M}(X)$ be a 2D manifold mesh with N vertices $X = \{x_i\}_{i=1}^N$ in \mathbb{E}^3 . Given an initial mesh $\mathcal{M}(X)$, we define the *extended CVT (ECVT) energy function* (under the usual L_2 norm $\|\cdot\|$) as

$$F_{\text{ECVT}}(X) = N \times \left(\sum_{i=1}^N \int_{y \in V_i \subset \mathcal{M}(X)} \|y - x_i\|^2 d\sigma \right), \quad (8)$$

where V_i is the restricted Voronoi cell of the vertex x_i to $\mathcal{M}(X)$ (cf. Section 2). In view of Eq. (7), we have introduced the number of vertices N in front of the CVT energy as a normalization factor to make the ECVT energy $F_{\text{ECVT}}(X)$ independent of the number of vertices (or seed points). Here, the mesh vertices of $\mathcal{M}(X)$ are at the same time the seed points for defining a Voronoi tessellation. As a consequence, the domain mesh $\mathcal{M}(X)$ for the ECVT energy $F_{\text{ECVT}}(X)$ in Eq. (8) is defined by the variable seed points X , therefore it changes when the seed points X are updated by optimization. This situation is different from the definition of the ordinary CVT energy in Eq. (1) for which the domain is fixed.

By the argument in Section 3.2, for a CVT X_0 , its ECVT energy $F_{\text{ECVT}}(X_0)$ in Eq. (8) is proportional to the squared surface area of the mesh $\mathcal{M}(X_0)$. Therefore, the minimization of $F_{\text{ECVT}}(X)$ implies the minimization of surface area. Furthermore, like the ordinary CVT energy, minimizing the ECVT energy of $\mathcal{M}(X)$ makes the mesh vertices uniformly distributed with optimized edge connectivity. Hence, the ECVT energy $F_{\text{ECVT}}(X)$ can be used to develop a method for generating minimal surfaces with high mesh quality. In the following, we will further extend the application of the ECVT energy to modeling CMC surfaces.

3.4 CVT-CMC energy

Given a mesh surface $\mathcal{M}(X)$ in \mathbb{E}^3 with mesh vertices $X = \{x_i\}_{i=1}^N$, the CVT-CMC energy of $\mathcal{M}(X)$ is defined by

$$\begin{aligned} F_{\text{CMC}}(X) &= F_{\text{ECVT}}(X) + t \times F_{\text{Vol}}(X) \\ &= N \times \left(\sum_{i=1}^N \int_{y \in V_i} \|y - x_i\|^2 d\sigma \right) + t \times \left(\sum_{i=1}^N \int_{y \in V_i} n_y \cdot x_i d\sigma \right), \end{aligned} \quad (9)$$

where n_y is the unit normal at a point y of a facet and $t \in \mathbb{R}$ is a parameter.

With a fixed parameter t , a fixed number of seed points N and a given boundary, we are going to show that minimizing $F_{\text{CMC}}(X)$ in Eq. (9) yields asymptotically a discrete CMC surface, using an interpretation similar to that for the CMC formulation in Eq. (2). Let $\mathcal{M}(X_0)$ denote a mesh that is a minimizer of $F_{\text{CMC}}(X)$. Then $\mathcal{M}(X_0)$ has the smallest CVT energy among all the meshes $\mathcal{M}(X)$ having the same volume as enclosed by $\mathcal{M}(X_0)$. Therefore, X_0 induces a CVT partition on the mesh $\mathcal{M}(X_0)$. Then, according to the proof in Section 3.2, since $F_{\text{ECVT}}(X_0)$ is asymptotically proportional to the squared surface area of $\mathcal{M}(X_0)$, $\mathcal{M}(X_0)$ has asymptotically the smallest squared surface area among all the meshes $\mathcal{M}(X)$ having the same volume as enclosed by $\mathcal{M}(X_0)$. Hence, $\mathcal{M}(X_0)$ is asymptotically a discrete CMC surface.

For the volume functional $F_{\text{Vol}}(X)$ in Eq. (9), we use the following formula for a closed mesh surface \mathcal{M} ,

$$F_{\text{Vol}}(X) = \sum_{i=1}^N \int_{y \in V_i} n_y \cdot x_i d\sigma = 3 \times \text{Vol}(X),$$

where $\text{Vol}(X)$ is the signed volume bounded by the surface. When \mathcal{M} is an open mesh surface with a boundary $\partial\mathcal{M}$, this formula gives the volume of the closed region bounded by \mathcal{M} and the cone surface defined by connecting the origin to the points on $\partial\mathcal{M}$. The fact that this value is not invariant under translation does not affect the minimization of the functional to yield a discrete CMC surface, as can be seen later in Eq. (11) that its gradient is invariant to translation.

Gradient formula. In order to minimize the CVT-CMC energy $F_{\text{CMC}}(X)$ using the L-BFGS method (cf. Section 4), we need to find its gradient formula. Keeping in mind that the domain $\mathcal{M}(X)$ changes with the seed points x_i , by straightforward derivation, we first find the gradient of F_{ECVT} to be

$$\begin{aligned} \frac{\partial F_{\text{ECVT}}}{\partial x_i} &= N \times (2m_i(x_i - c_i) \\ &+ \frac{1}{24} \sum_j (\|x_i - v_{j1}\|^3 n_{j1} + \|x_i - v_{j2}\|^3 n_{j2})), \end{aligned} \quad (10)$$

where m_i and c_i are the mass (i.e., area) and the centroid of the Voronoi cell of the vertex x_i , respectively, j is an index of a triangle face T_j in the 1-ring neighborhood of x_i , v_{j1} and v_{j2} are the other two vertices of T_j , and n_{j1} and n_{j2} are the unit normal vectors of the edges $x_i v_{j1}$ and $x_i v_{j2}$ in the plane of T_j (see the inset on the right in which the Voronoi cell of x_i is colored). The gradient formula in Eq. (10) is derived by following the idea of the CVT gradient derivation in [Du et al. 1999]. Specifically, we take $F_{\text{ECVT}}(X)$ in the form $F_{\text{ECVT}}(X; \mathcal{M}(X))$, meaning that the function depends on the seeds X directly as well as the domain $\mathcal{M}(X)$, while $\mathcal{M}(X)$ in turn also depends on X . We then differentiate it with respect to X and the compound variable $\mathcal{M}(X)$. The differentiation with respect to X yields the standard CVT gradient (i.e., the first term in Eq. (10)), and the differentiation with respect to $\mathcal{M}(X)$ results in the second term.

The gradient of the CVT-CMC energy is then

$$\frac{\partial F_{\text{CMC}}}{\partial x_i} = \frac{\partial F_{\text{ECVT}}}{\partial x_i} + \frac{\partial F_{\text{Vol}}}{\partial x_i} = \frac{\partial F_{\text{ECVT}}}{\partial x_i} + t \sum_j S_j n_j, \quad (11)$$

where S_j and n_j are the area and the unit normal vector of the j -th triangle face in the 1-ring neighborhood of the vertex x_i , respectively.

3.5 Shape control

Interpretation of parameter t . The parameter t in the CVT-CMC energy function in Eq. (9) is important for controlling the shape of a CMC surface. Since there is Eq. (6) for the relationship between the CVT energy and the domain area, for a minimizer of the CVT-CMC energy functional, we have $2\sigma A \nabla A = -t \nabla \text{Vol}$, where A is the mesh area, Vol is the signed volume bounded by the mesh and $\sigma = \tau/\tau'^2$ is the same constant coefficient as in Eq. (6). It is known that when $\nabla A = -\lambda \nabla \text{Vol}$, $-\lambda$ is the mean curvature H [Polthier and Rossman 2002], and is also the gas pressure if the surface is regarded as a soap bubble that assumes a CMC shape naturally [Brakke 1992]. So, as a physical interpretation, $t = 2\sigma \lambda A$ is the total force exerted on the mesh surface. It is more convenient and robust to control the shape using the parameter t than using the mean curvature, as we will see next.

Shape control using parameter t . During an interactive form finding process, it is important that one is able to explore easily the entire series of CMC surfaces having the same boundary constraints. Consider the process of inflating a spherical cap with the same ring boundary, as shown in Fig. 2(a). Fig. 2(b) shows that the mean curvature of the caps is not monotonic against the increasing volume, and a single mean curvature value may correspond to two distinct CMC surfaces. This lack of one-to-one correspondence indeed causes difficulties for some methods, such as Surface Evolver [Brakke 1992; Brakke 2012], which use λ (i.e., mean curvature) as a shape control parameter. In fact, by simply manipulating the mean curvature in this example, it is not possible for Surface Evolver to start from the flat spherical cap on the left of Fig. 2(a) and generate those surfaces on the right beyond the semi-sphere (for which the maximum mean curvature is attained).

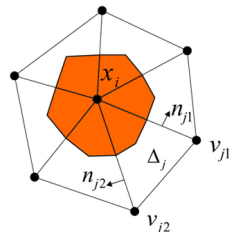
In contrast, our method provides an intuitive and robust tool for interactive shape exploration of CMC surfaces by using t as the shape control parameter. For example, our method easily produces the entire sequence of CMC surfaces in Fig. 2(a) by simply increasing t monotonically, as shown in Fig. 2(c). Figs. 1 and 15 give several examples of generating a sequence of discrete CMC surfaces by varying the control parameter t using our method.

It is also worth noting that in order to obtain a control parameter that is linear to mean curvature, one may instead use the functional $\sqrt{F_{\text{ECVT}}(X)} + t \times F_{\text{Vol}}(X)$, since according to Eq. (7), $\sqrt{F_{\text{ECVT}}(X)}$ is proportional to surface area asymptotically. Under this slightly modified energy functional, the parameter t is then proportional to mean curvature.

4 Discrete CMC Surface Modeling

We compute a discrete CMC surface as a minimizer of the CVT-CMC energy via an optimization framework. Starting from an initial mesh complying with some given boundary conditions, at each iteration, we minimize the CVT-CMC energy to yield new vertex positions. A new mesh is then obtained by updating mesh connectivity. The iterations proceed until convergence.

Optimization. We apply the L-BFGS method [Liu and Nocedal 1989] to minimize the CVT-CMC energy $F_{\text{CMC}}(X)$ in Eq. (9). It is an efficient implementation of a quasi-Newton method with reasonable space consumption, and has demonstrated superior convergence than gradient descent in the setting of minimizing the C^2



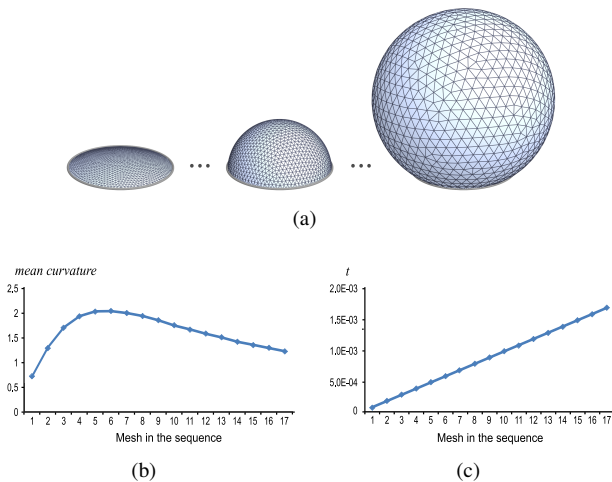


Figure 2: (a) A sequence of CMC surfaces with increasing volume and the same ring boundary. The middle CMC surface has the maximum mean curvature. (b) The mean curvature of the sequence is not monotonic and therefore methods relying on direct manipulating the mean curvature for shape control, such as Surface Evolver, will have difficulty to go beyond the middle cap to the right one. (c) Our method can generate the entire sequence easily by increasing t monotonically.

CVT energy [Liu et al. 2009]. Although the global smoothness of the CVT-CMC energy has not been established, we observe that the L-BFGS method is much faster than the gradient descent method in minimizing the CVT-CMC energy. As a quasi-Newton method, the L-BFGS method requires only evaluation of the energy function and its gradient (Eq. (11)).

Mesh update. The computation of the ECVT energy in Eq. (8) requires the restricted Voronoi diagram (RVD) of a mesh. Our special setting of having mesh vertices as the seed points admits a more efficient RVD implementation than the general RVD computation involving 3D Delaunay construction and polygon clipping by Yan et al. [2009]. Here, whenever a new set of vertex positions are obtained, we perform extrinsic edge flipping to update the combinatorics of the mesh until the local Delaunay condition that “every pair of opposite angles of two adjacent triangles sum up to no more than π ” is met. This is similar to the Delaunay mesh condition by Dyer et al. [2007], which also implies that all facet angles are acute for reasonably good vertex distribution. In this way, we may consider a Voronoi cell to involve only the 1-ring neighbor facets of a vertex, with its boundary connecting facet circumcenters and edge mid-points, and therefore have closed form expression to be computed very efficiently.

The edge flipping procedure may encounter unflippable edges which if flipped, will coincide with some existing edges in the mesh. Unflippable edges are regarded in [Dyer et al. 2007] as a sign of insufficient sampling rate, and refinement is needed to increase the number of samples. In our algorithm, however, unflippable edges are treated as the existence of singularities due to extreme curvature change which may occur naturally in the evolution process of a CMC surface computation. There are only two possible cases of unflippable edges, namely 2-exposed and 3-exposed, as identified in [Dyer et al. 2007]. The number n in n -exposed stands for the number of facets of the flip tetrahedron (i.e., one that is defined by the unflippable edge and its opposite edge) that are mesh triangles. Fig. (3) depicts how we handle the two cases as case (i)

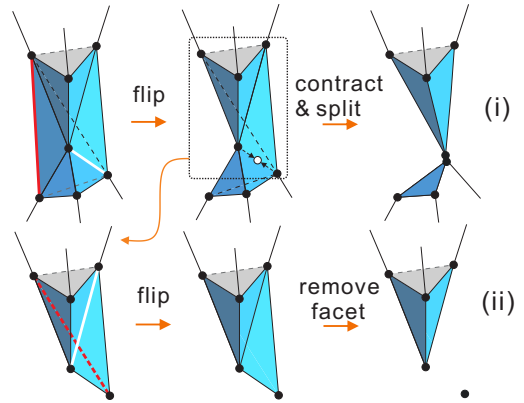


Figure 3: The handling of two possible cases of unflippable edges. The unflippable edges (in red) are flipped to their opposite ones (in white) as usual. In case (i), the nonmanifold edge is contracted and the mesh is split into two components; in case (ii), a nonmanifold facet is removed. After the procedure, the mesh remains a 2D manifold.

and case (ii), respectively. Our algorithm flips the unflippable edges to their opposite edges as usual in the edge flipping procedure, thus creating nonmanifold edges. We then apply mesh surgery to remove the nonmanifold situations accordingly. It is possible that the aforementioned local Delaunay condition is slightly violated at the modified edges, which, however, does not affect the overall optimization. It is also observed that due to extreme curvature at singularity, triangles have to be slim around a nonmanifold edge, and hence the 2-exposed case can be treated as a 3-exposed case (see the upper portion, in dashed box, of the middle configuration in case (i) of Fig. (3)). Handling this pseudo 3-exposed case will also result in splitting the mesh into two components, just as what one should obtain in case (i). Therefore, we may even skip the “contract & split” step for the 2-exposed cases in our implementation.

Use of the parameter t . Given a boundary and an initial mesh that is not necessarily a CMC surface, we estimate an initial value t_0 of the parameter t by computing the ratio of the gradients of the ECVT energy to the volume functional on the initial mesh. This is done by summing up

$$t_i = -\left\langle \frac{\partial F_{ECVT}}{\partial x_i}, \frac{\partial F_{Vol}}{\partial x_i} \right\rangle / \left\| \frac{\partial F_{Vol}}{\partial x_i} \right\|^2$$

where \langle , \rangle is the inner product, over all the vertices x_i . Then the initial mesh will be optimized into a CMC surface dictated by t_0 , which is to be used as a reference surface. After that, the user may adjust the value of t to explore a range of CMC surfaces having the same boundary but of different shapes.

5 Results

5.1 Validation and comparisons

We use examples of both minimal surfaces and CMC surfaces to demonstrate the validity and effectiveness of our method in terms of approximation quality and mesh quality. In each example, we use an initial mesh having a topology similar to the final mesh and at the same time complying with the given boundary curves. We start by evaluating our results using two well-known CMC surfaces, the catenoid and the unduloid.

Approximation to analytical surfaces. The *catenoid* is one of the earliest found minimal surfaces and is the soap film developed between two coaxial circular rings when moving them apart slowly [Osserman 2002]. We compare the approximation of the catenoid surface computed by our method with mean curvature flow (MC flow) using the cotangent formula by Pinkall and Polthier [1993] (Fig. 4). Our method produces a discrete minimal surface with smaller area than MC flow, even though MC flow directly minimizes mesh area. This testifies the importance of mesh quality on minimizing mesh area. Our result is also a close approximation to the analytical catenoid (a maximum vertex distance of 0.013 to the catenoid given that the minimum radius of its neck is 1). It is also possible to have the CVT-CMC optimization followed by an MC flow to further reduce mesh area; for example, by taking our resulting catenoid as input, MC flow produces a slight reduction to the mesh area by 0.02% (Fig. 4(d)).

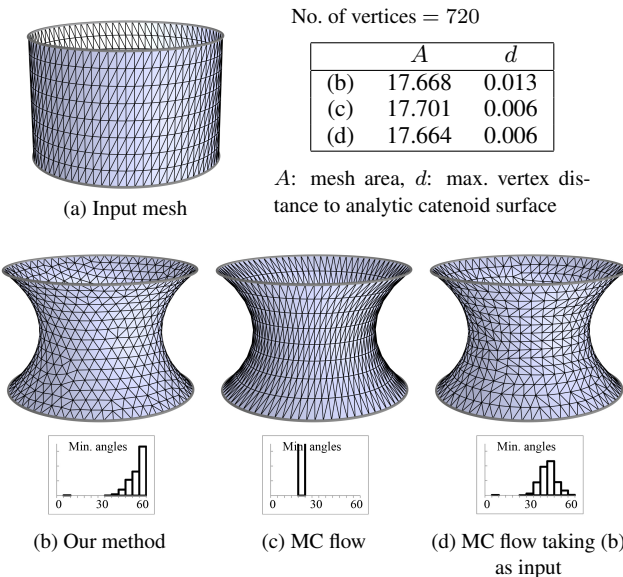


Figure 4: Discrete catenoid surfaces. The neck has a minimum radius equal to 1. The table gives the area of the resulting meshes and the maximum distance of vertices to the analytic catenoid surface. Our method produces a high quality mesh with smaller area than using mean curvature flow (MC flow). By taking our result as an initial mesh, MC flow (which directly minimizes mesh area) only improves the mesh area slightly by 0.02%.

An *unduloid* is a CMC surface which is a surface of revolution generated by the path of a focus of an ellipse rolling on the axis of revolution and looks like blobs of viscous liquid [Hadzhilazova et al. 2007]. We compute a discrete unduloid surface with a specific volume and determine its area and its maximum distance to the corresponding analytical unduloid surface (Fig. 5). We compare our result against that of Surface Evolver [Brakke 1992], a program that generates CMC surfaces by minimizing mesh area with a volume constraint. The output mesh generated by our method is used as an input to Surface Evolver, as Surface Evolver does not optimize mesh connectivity and its performance depends therefore on the input mesh quality. In this example, Surface Evolver only slightly reduced the area by 0.02%.

Remark: In practice we work with meshes of a limited number of vertices to approximate CMC surfaces, and the least number of vertices with which we may get a good approximation also depends on the specific shape of a surface. Generally speaking, as the number

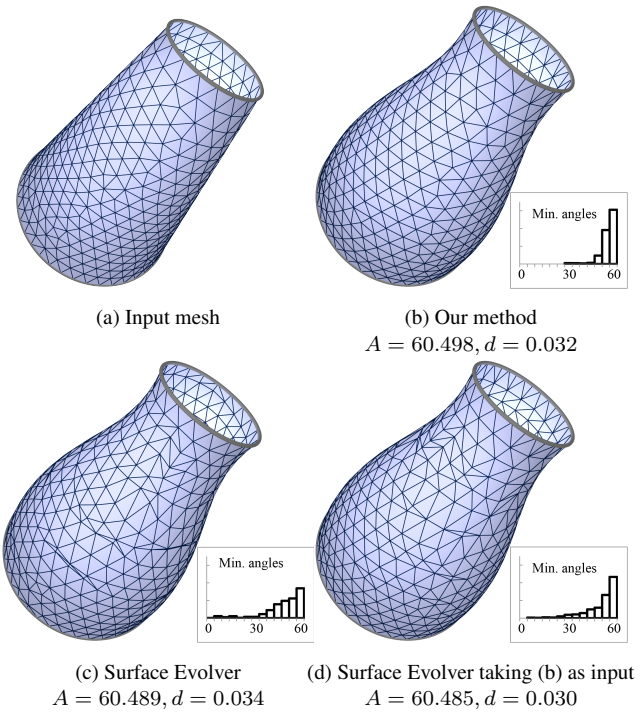


Figure 5: Discrete unduloid surfaces. A: Mesh area; d: maximum vertex distance to the analytical unduloid surface. Surface Evolver only improves the mesh area of our result slightly by 0.02%.

of vertices increases, we get better approximations. However, it is nontrivial to examine asymptotic behaviors merely using numerical experiments, as there is always the difficulty of finding the global minimum of the energy functional.

Mesh quality comparisons. Fig. 6 shows another example of a minimal surface with a saddle-shaped boundary, with an initial mesh containing a sharp edge. Pinkall and Polthier’s method [1993] distorts the mesh severely due to its lack of ability to re-establish vertex connectivity. We also compare against Bobenko [2007], a Delaunay augmented version of Pinkall and Polthier’s method that allows mesh connectivity change. Both Bobenko’s and our methods can handle the abrupt change towards the resulting surface which has a very different shape from the input. However, our method produces a result of the best mesh quality with the smallest area among all the results.

Comparisons with Surface Evolver. Fig. 7 shows two discrete CMC surfaces with the same volume and boundary curve computed by our method and Surface Evolver. Our method results in a high quality discrete CMC mesh with an area close to that of Surface Evolver. Taking our resulting discrete CMC surface as the initial mesh, Surface Evolver can further reduce the mesh area by 0.2% when the number of vertices (N) is 100, and this reduction decreases linearly as N increases (Fig. 7(c)). This indicates that our method performs as good as minimizing mesh area directly, while offering superior mesh quality.

We also compute the discrete mean curvature values by the cotangent mean curvature normal method [Meyer et al. 2003]. It is noted that an ordinary optimization routine in general yields a local minimum only (since the CVT-CMC energy is highly nonconvex). By using a simulated annealing technique [Pardalos and Romeijn

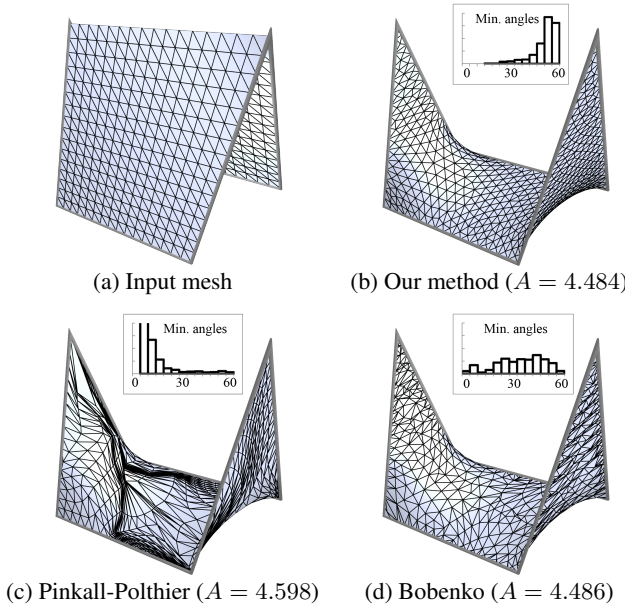


Figure 6: Computing a discrete minimal surface with a saddle-shaped boundary. Our method yields the minimum mesh area and the best mesh quality.

2002] for global optimization, we obtain an approximation to the global minimizer of the CVT-CMC energy. Fig. 7(d) shows that the mean curvature distribution of our result by global optimization is comparable to that of Surface Evolver. We also note that the variations of the mean curvature value of our result appear mostly at vertices that are close to the boundary or at irregular vertices whose valence is not six (Fig. 7(a)). This phenomenon can be accounted for by the fact that the asymptotic equipartition property of CVT (G1) does not generally hold at the boundary; also, we observe that on our resulting mesh, which consists mostly of regular triangles, the discrete operator for approximating mean curvature is more accurate at vertices of valence six than at other vertices.

Fig. 8 shows a comparison of our method with Surface Evolver on generating several discrete CMC surfaces in terms of mesh quality and robustness. It can be seen that the resulting mesh by Surface Evolver contains many slim and long triangles, while our method yields much better results in terms of mesh quality. Surface Evolver supports remeshing interlaced with optimization by means of the operations “Equiangulation” for mesh combinatoric update and “Vertex Averaging” for Laplace smoothing on the mesh. With remeshing, Surface Evolver generates meshes with better quality and a smoother shape (Model I of Fig. 8). However, the Laplace smoothing in the interlaced optimization does not reduce the energy used by Surface Evolver which renders the process non-converging. Indeed, in some cases, vertices are found to oscillate between being smoothed or reducing surface energy. Model II is a typical scenario in which the interlaced iterations do not converge and the mesh expands infinitely. Fig. 8(**) is an intermediate mesh that will eventually blast, so the final result for Surface Evolver in this case is not available. Our method, combining area minimization as well as remeshing in the CVT-CMC energy, ensures a robust modeling process that produces high quality CMC meshes.

Comparison with PDE based method. We also compare our method with the PDE based approach by Xu and Zhang [2008], where geometric differential equations are solved with a finite difference scheme using quadratic fitting for each element. The re-

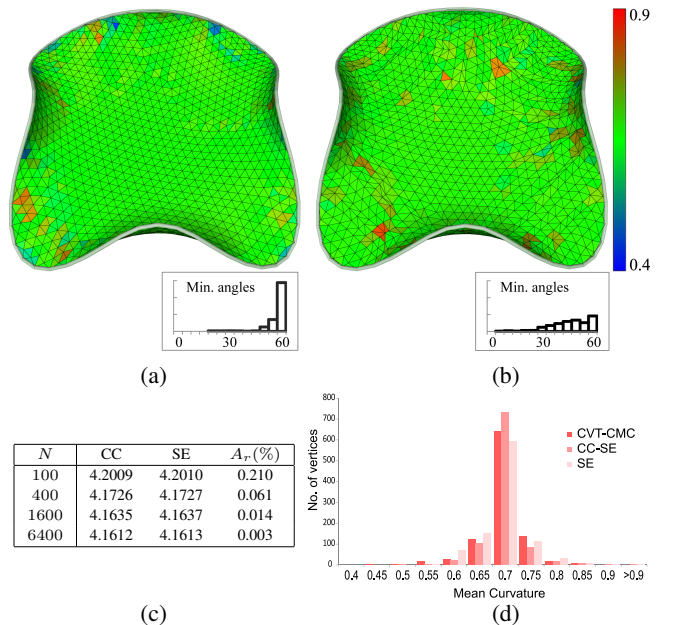


Figure 7: Discrete CMC surfaces with same volume and boundary curve generated by (a) our method; and (b) Surface Evolver, and color coded with discrete mean curvatures by the cotangent formula. (c) Mesh area versus number of vertices (N) by our method (CC), Surface Evolver (SE) and the area reduction (A_r) in % by Surface Evolver taking our result as input. (d) The mean curvature distribution of the resulting mesh by our method (CVT-CMC), Surface Evolver (SE), and Surface Evolver taking our result as input (CC-SE).

sults are shown in Fig. 9. It can be observed that the PDE based approach is sensitive to the input triangulation, whose quality, if not good enough, will cause the resulting surface to have not only slim triangles but also a larger mean curvature deviation (Fig. 9(c)). Remeshing such a result improves the mesh quality; at the same time, however, it worsens the mean curvature measure as is shown in (d).

5.2 Robustness upon topological change

When the two rings of a catenoid soap film are moved further apart, the neck of the catenoid will gradually become narrower until when the ring separation/radius ratio reaches the critical value 1.33, upon which the neck breaks up and the catenoid splits into two disks. Fig. 10 depicts how this phenomenon can be captured by our method by simulating the evolution of the catenoid into two disks. This sequence of catenoid surfaces is generated by stretching the current catenoid with rings moved further apart, and then using the stretched mesh as an input to produce the next catenoid.

Throughout the simulation of the evolution of the catenoid soap film, there is a transition in which the 1-sheet input mesh results in an output with two disks. The splitting of an input mesh is shown in Fig. 11 in which we take two coaxial rings whose separation/radius ratio is larger than the critical value 1.33 as the boundary for constructing a minimal surface. The minimal surface is therefore expected to be of two disks, each bounded by one of the rings. Our method can drive the evolution of the cylinder and split it into two pieces naturally, via the edge flipping operation described in Section 4.

The split of a catenoid can also be dealt with by Chopp [1993];

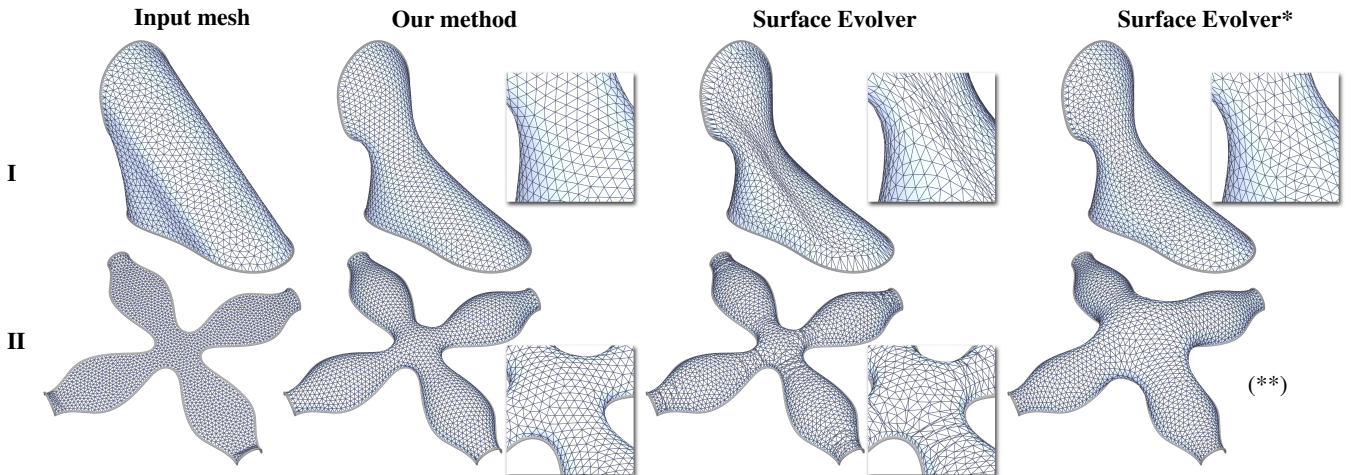


Figure 8: Comparison with *Surface Evolver* for two CMC surfaces. *Surface Evolver** is the result of *Surface Evolver* with remeshing by the “Equiangulation” and “Vertex Averaging” operations. Our method has a robust modeling process that yields higher mesh quality than *Surface Evolver*. The remeshing operations of *Surface Evolver* can help improve its resulting mesh quality as shown in Model I; however, in some cases, *Surface Evolver* with remeshing does not converge as is shown in (**) of Model II which is an intermediate result only.

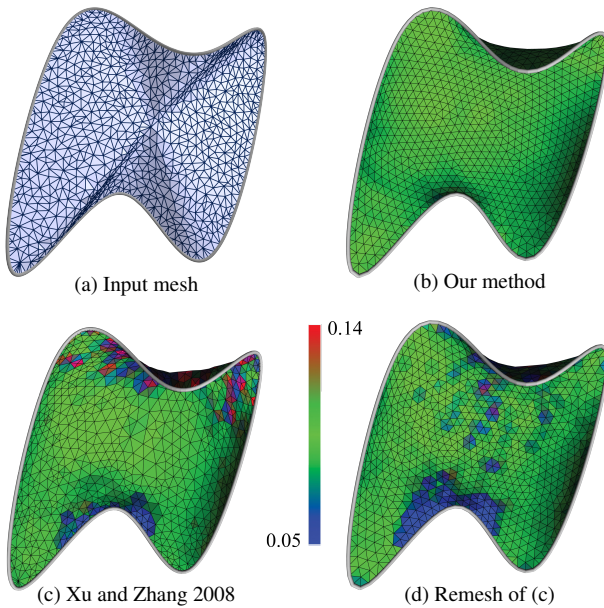


Figure 9: Comparison with Xu and Zhang [2008], a PDE based approach, with resulting meshes color-coded according to mean curvature. (b) Our method generates a discrete CMC surface with a superior mesh quality over the PDE method. (c) The blue part at the bottom of the PDE result indicates a defective region where the mean curvature is comparatively lower. (d) A remesh of the PDE result improves the mesh quality but worsens the mean curvature measure.

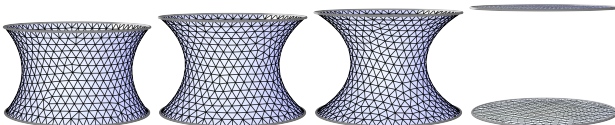


Figure 10: The evolution of a catenoid into two disks simulated using our method.

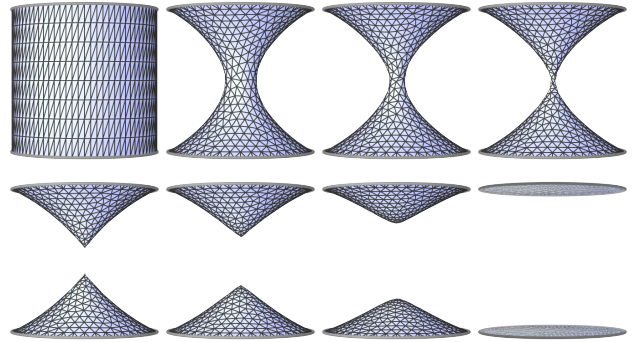


Figure 11: The process of splitting a 1-sheet input mesh into an output of two disks. Intermediate meshes in our optimization are shown from top-left (the initial mesh) to bottom-right (the final result). Our method can naturally handle topological change of the mesh during the optimization process.

however, the method is level set-based and therefore does not work for those minimal surfaces without a level set representation, such as the Möbius band. A Möbius band soap film developed between a double loop boundary curve can turn into a two-sided minimal surface solution when the loop is gradually pulled apart and untwisted [Goldstein et al. 2010]. This interesting process can be simulated robustly with our method, as is shown in Figure 12.

5.3 Boundary handling

There are different types of boundaries or geometric constraints for CMC surfaces encountered in applications. These include fixed boundaries, free boundaries constrained on a fixed surface, free boundary curve segments with fixed length, and nonmanifold edges shared by more than two surface sheets. In the following, we will discuss how these different cases can be treated in our modeling framework.

Fixed boundary. A fixed boundary of a CMC surface does not move when the surface evolves to adopt different mean curvature values. Given a fixed boundary curve, the user may define an initial

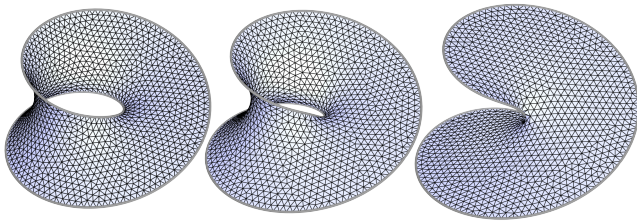


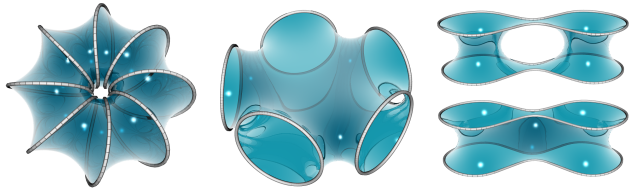
Figure 12: A one-sided Möbius surface evolves to two-sided minimal surface by gradually pulling apart and untwisting the double loop boundary curve.

simple shape interpolating the boundary, and then apply the optimization scheme to compute a CMC surface. Note that sufficiently many mesh vertices are necessary for well approximating a smooth surface. The number of mesh vertices can be added or removed progressively to balance computational efficiency and approximation accuracy. Fig. 13 shows some minimal surfaces with fixed boundaries and Fig. 14 shows examples of discrete CMC surfaces representing CAD models, which are created with our method. More examples of CMC surfaces with fixed boundary generated by a varying control parameter t are shown in Fig. 15.

Boundary mesh vertices are determined via relaxation and re-projection as follows. All the boundary vertices are first relaxed to become interior vertices and therefore will undergo the CVT-CMC optimization. After optimization, those interior vertices whose Voronoi cells intersect the boundary curve will be re-projected onto the boundary curve. Such a relaxation plus re-projection step is also applied if the number of boundary vertices does not match well with the number of interior vertices during the evolution of a CMC surface, either when there is a radical change of the surface area or when there are many mesh vertices being added or removed [Yan et al. 2010].

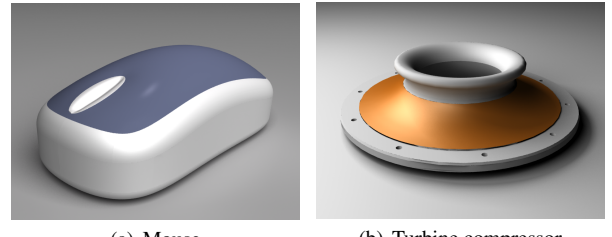
Free boundary. We consider two types of free boundaries. The first type are those boundary curves having two fixed endpoints and a fixed length, but are free to vary in 3D; flexible cable lines of tensile membranes are such examples. A tensile membrane structures with this type of free boundary modeled with our method is shown in Fig. 16. The other type refers to a boundary curve of a CMC surface that is constrained to lie on a given surface, as in the case of soap bubbles attached to a table surface. The cluster of bubbles on a flat surface shown in Figure 17(a) is an example of a CMC surface with free boundaries modeled using our method. Note that a CMC surface may have fixed boundaries and free boundaries at the same time. The treatment of free boundaries is similar to fixed boundaries, except that now the boundary mesh vertices are allowed to move when the shape of the CMC surface changes, subject to their specific constraints.

Nonmanifold boundary. A nonmanifold boundary is a feature curve incident to three or more CMC surface sheets, as in the case of the soap bubbles shown in Fig. 17. When three sheets share a curve, which is called a *Plateau border*, they form three pairwise angles of 120 degrees along the curve [Taylor 1976]. Our investigation shows that for mesh vertices on a nonmanifold boundary, locally minimizing the surface area of the strip of triangles incident to the boundary vertices produces smoother boundary curve than using the CVT-CMC energy function; this is probably due to the reason that the ECVT energy needs a larger region to distribute the vertices evenly. Therefore, we adopt the strategy of alternatingly optimizing the CVT-CMC energy of the interior vertices while fixing the boundary vertices, and minimizing the surface area of the



(a) Circular helical (b) Fivenoid (c) Two rings

Figure 13: Some minimal surfaces with different boundaries generated by our method. The two minimal surfaces in (c) are of the same boundary but have different topologies.



(a) Mouse (b) Turbine compressor

Figure 14: CAD models in mesh. The blue cover in (a) and the brown neck in (b) are CMC surfaces computed by our method, given the boundaries fixed as input. Original shapes from AIM@Shape.

strip of triangles incident to the free boundary vertices while fixing the interior vertices. Fig. 17 shows our results of computing soap bubbles with free and nonmanifold boundaries.

6 Conclusion

We presented a new method for discrete CMC surface modeling which takes into account mesh quality while minimizing surface area with a volume constraint. We proposed the extended centroidal Voronoi tessellation (ECVT) energy and showed that the energy can govern the minimization of surface area when the domain is allowed to vary. By optimizing a new CVT-CMC energy which combines the ECVT energy and the volume functional, one can generate a discrete CMC surface with high mesh quality in a unified formulation. Our method also provides a robust shape-control parameter that supports interactive shape exploration.

A limitation of our current method is that it assumes a constant distribution of vertices over the mesh, which means that the number of vertices in a certain part of the mesh does not depend on

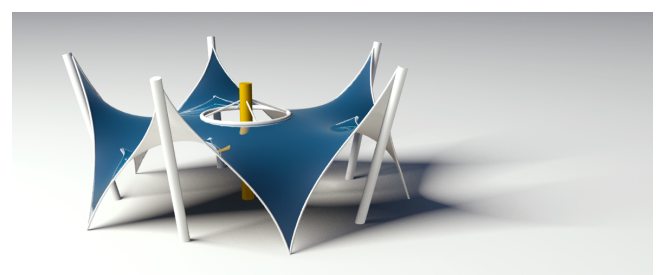


Figure 16: A tensile membrane structure with cables and fixed boundaries.

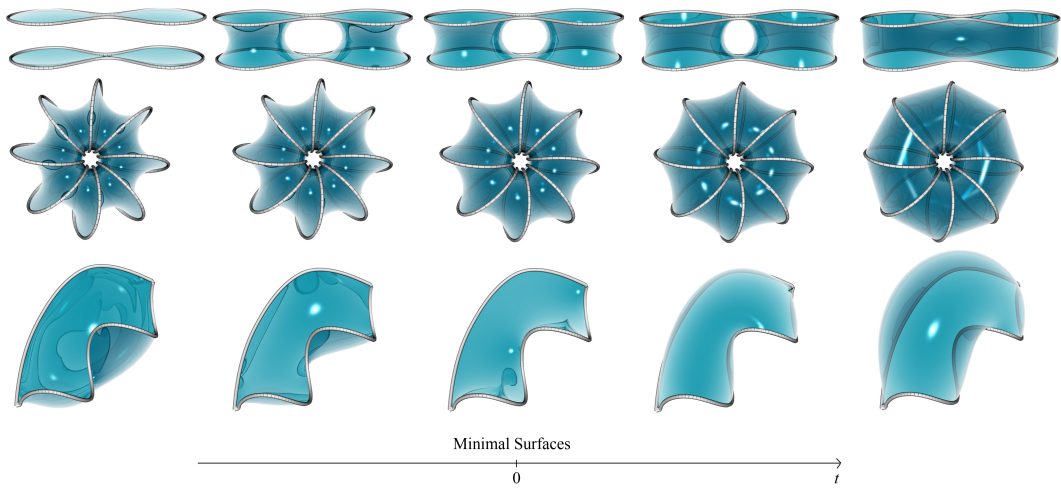


Figure 15: More examples of a sequence of CMC surfaces of the same boundary generated by varying the control parameter t using our method. The surfaces for which $t = 0$ are the minimal surfaces.

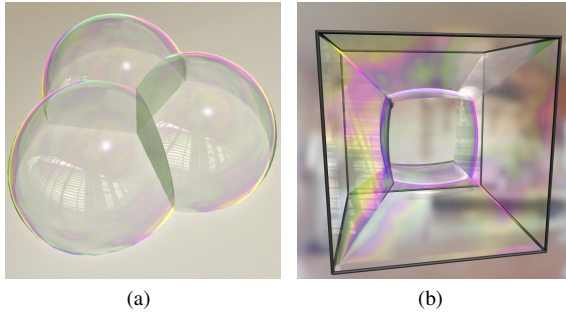


Figure 17: Examples of bubbles with free and nonmanifold boundary conditions.

the local geometric properties, e.g., surface curvature. For surfaces with many features, a large number of vertices will be needed for smooth modeling of regions of high curvatures. Future research is therefore needed to incorporate adaptive vertex distribution to further improve the mesh quality.

Acknowledgments

We would like to thank the anonymous reviewers for their helpful comments. This project is supported in part by NSFC (11031007), the State Key Program of NSFC Project (60933008), the Major International (Regional) Joint Research Project of NSFC (61020106001), National Basic Research Program of China (2011CB302400) and the Research Grant Council of Hong Kong (718209 and 718010), Einstein Foundation Program of Berlin Mathematical School, Beijing Computational Science Research Center and DFG Research Center MATHEON. We also thank Qin Zhang and Guoliang Xu for providing their results. The original CAD model used in Fig. 14 is obtained from the Aim@Shape repository; the turbine compressor and the mouse models are courtesy of INRIA and LAB3S, respectively.

References

- BOBENKO, A. I., AND SPRINGBORN, B. A. 2007. A discrete Laplace-Beltrami operator for simplicial surfaces. *Discrete & Computational Geometry* 38, 4, 740–756.
- BRAKKE, K. 1992. The Surface Evolver. *Experimental Mathematics* 1, 2, 141–165.
- BRAKKE, K., 2012. The Surface Evolver, version 2.30. <http://www.susqu.edu/brakke/evolver/evolver.html>, May.
- BREW, J., AND LEWIS, W. 2003. Computational form-finding of tension membrane structures – Non-finite element approaches: Part 1. Use of cubic splines in finding minimal surface membranes. *International journal for numerical methods in engineering* 56, 5, 651–668.
- BREW, J., AND LEWIS, W. 2003. Computational form-finding of tension membrane structures – Non-finite element approaches: Part 2. Triangular mesh discretization and control of mesh distortion in modelling minimal surface membranes. *International Journal for Numerical Methods in Engineering* 56, 5, 669–684.
- CHOPP, D. 1993. Computing minimal surfaces via level set curvature flow. *Journal of Computational Physics* 106, 77–77.
- DU, Q., FABER, V., AND GUNZBURGER, M. 1999. Centroidal Voronoi tessellations: Applications and algorithms. *SIAM Review* 41, 4, 637–676.
- DU, Q., GUNZBURGER, M., AND JU, L. 2003. Constrained centroidal Voronoi tessellations for surfaces. *SIAM Journal on Scientific Computing* 24, 5, 1488–1506.
- DU, Q., GUNZBURGER, M., AND JU, L. 2010. Advances in studies and applications of centroidal Voronoi tessellations. *Numer. Math. Theor. Appl.* 3, 119–142.
- DYER, R., ZHANG, H., AND MÖLLER, T. 2007. Delaunay mesh construction. In *Proceedings of the fifth Eurographics Symposium on Geometry Processing*, Eurographics Association, Aire-la-Ville, Switzerland, 273–282.
- DZIUK, G., AND HUTCHINSON, J. E. 2006. Finite element approximations to surfaces of prescribed variable mean curvature. *Numerische Mathematik* 102, 611–648. 10.1007/s00211-005-0649-7.

- GERSHO, A. 1979. Asymptotically optimal block quantization. *IEEE Transactions on Information Theory* 25, 4, 373–380.
- GOLDSTEIN, R., MOFFATT, H., PESCI, A., AND RICCA, R. 2010. Soap-film Möbius strip changes topology with a twist singularity. *Proceedings of the National Academy of Sciences* 107, 51, 21979.
- GRUBER, P. 2001. Optimal configurations of finite sets in Riemannian 2-manifolds. *Geometriae Dedicata* 84, 271–320. 10.1023/A:1010358407868.
- HADZHILAZOVA, M., MLADENOV, I., AND OPREA, J. 2007. Unduloids and their geometry. *Archivum Mathematicum* 43, 5, 417–429.
- KAPOULEAS, N. 1990. Complete constant mean curvature surfaces in Euclidean three-space. *The Annals of Mathematics* 131, 2, 239–330.
- LIU, D., AND NOCEDAL, J. 1989. On the limited memory bfgs method for large scale optimization. *Mathematical programming* 45, 1, 503–528.
- LIU, Y., WANG, W., LÉVY, B., SUN, F., YAN, D.-M., LU, L., AND YANG, C. 2009. On centroidal Voronoi tessellation—energy smoothness and fast computation. *ACM Trans. Graph.* 28, 4, 1–17.
- MEYER, M., DESBRUN, M., SCHRÖDER, P., AND BARR, A. H. 2003. Discrete differential-geometry operators for triangulated 2-manifolds. In *Visualization and Mathematics III*, H.-C. Hege and K. Polthier, Eds. Springer-Verlag, Heidelberg, 35–57.
- OBERKNAPP, B., AND POLTHIER, K. 1997. An algorithm for discrete constant mean curvature surfaces. In *Visualization and Mathematics*, H.-C. Hege and K. Polthier, Eds. Springer Verlag, Heidelberg, 141–161.
- OSSERMAN, R. 2002. *A survey of minimal surfaces*. Dover Pubns.
- PARDALOS, P., AND ROMEIJN, H. 2002. *Handbook of global optimization. Volume 2*. Kluwer.
- PINKALL, U., AND POLTHIER, K. 1993. Computing discrete minimal surfaces and their conjugates. *Experimental mathematics* 2, 1, 15–36.
- POLTHIER, K., AND ROSSMAN, W. 2002. Discrete constant mean curvature surfaces and their index. *J. reine angew. Math.*, 549, 47–77.
- SMITH, J. 2003. *Three Applications of Optimization in Computer Graphics*. PhD thesis, Robotics Institute, Carnegie Mellon University, Pittsburgh, PA.
- TAYLOR, J. E. 1976. The structure of singularities in soap-bubble-like and soap-film-like minimal surfaces. *The Annals of Mathematics* 103, 3, 489–539.
- XU, G., AND ZHANG, Q. 2008. A general framework for surface modeling using geometric partial differential equations. *Computer Aided Geometric Design* 25, 3, 181–202.
- XU, G., PAN, Q., AND BAJAJ, C. 2006. Discrete surface modelling using partial differential equations. *Computer Aided Geometric Design* 23, 2, 125–145.
- YAN, D., LÉVY, B., LIU, Y., SUN, F., AND WANG, W. 2009. Isotropic remeshing with fast and exact computation of restricted Voronoi diagram. In *Computer graphics forum*, vol. 28, Wiley Online Library, 1445–1454.
- YAN, D., WANG, W., LÉVY, B., AND LIU, Y. 2010. Efficient computation of 3D clipped Voronoi diagram. *Advances in Geometric Modeling and Processing*, 269–282.